J Mater Sci: Mater Med (2013) 24:1659–1670
DOI 10.1007/s10856-013-4934-1

A novel porous scaffold fabrication technique for epithelial and endothelial tissue engineering

Kevin J. McHugh · Sarah L. Tao · Magali Saint-Geniez

Received: 7 February 2013 / Accepted: 18 April 2013 / Published online: 27 April 2013

Abstract Porous scaffolds have the ability to minimize transport barriers for both two- (2D) and three-dimensional tissue engineering. However, current porous scaffolds may be non-ideal for 2D tissues such as epithelium due to inherent fabrication-based characteristics. While 2D tissues require porosity to support molecular transport, pores must be small enough to prevent cell migration into the scaffold in order to avoid non-epithelial tissue architecture and compromised function. Though electrospun meshes are the most popular porous scaffolds used today, their heterogeneous pore size and intense topography may be poorly-suited for epithelium. Porous scaffolds produced using other methods have similar unavoidable limitations, frequently involving insufficient pore resolution and control, which make them incompatible with 2D tissues. In addition, many of these techniques require an entirely new round of process development in order to change material or pore size. Herein we describe "pore casting," a fabrication method that produces flat scaffolds with deterministic pore shape, size, and location that can be easily altered to accommodate new materials or pore dimensions. As proof-of-concept, pore-cast poly(ε-caprolactone) (PCL) scaffolds were fabricated and compared to electrospun PCL in vitro using canine kidney epithelium, human colon epithelium, and human umbilical vein endothelium. All cell types demonstrated improved morphology and function on pore-cast scaffolds, likely due to reduced topography and universally small pore size. These results suggest that pore casting is an attractive option for creating 2D tissue engineering scaffolds, especially when the application may benefit from well-controlled pore size or architecture.

K. J. McHugh · S. L. Tao
The Charles Stark Draper Laboratory, Inc., 555 Technology Square, Cambridge, MA 02136, USA

K. J. McHugh
Department of Biomedical Engineering, Boston University, 44 Cummington St., Boston, MA 02115, USA

K. J. McHugh · M. Saint-Geniez (✉)
Schepens Eye Research Institute, 20 Staniford St., Boston, MA 02114, USA
e-mail: magali_saintgeniez@meei.harvard.edu

Present Address:
S. L. Tao
CooperVision, Inc., 5870 Stoneridge Dr., Pleasanton, CA 94588, USA

M. Saint-Geniez
Department of Ophthalmology, Harvard Medical School, 243 Charles Street, Boston, MA 02114, USA

1 Introduction

Tissue engineering has the potential to revolutionize medicine by creating functional tissues. Producing these tissues frequently requires the use of scaffolds to support cell adhesion, proliferation, and organization. In particular, porous scaffolds have gained popularity for their ability to facilitate the transport of metabolites and waste which is ubiquitously required for all tissues. However, tissue engineers must also consider the effect of porous scaffold architecture on physical cell-surface interactions which can strongly regulate behavior [1–4]. As a result, pores appropriate for three-dimensional (3D) tissues may be inappropriate for two-dimensional (2D) tissues such as epithelium and endothelium.

Native epithelium forms a largely 2D monolayer or stratified multilayer which acts as a physical barrier and

regulator of transport between adjacent body compartments [5]. To retain this function, implantable epithelial scaffolds must be permeable, but also prevent cell invasion that would otherwise lead to abnormal tissue morphology and impaired function [3, 6]. Pores in solid materials are capable of providing this type of selective barrier, but only if they are sufficiently small to prevent cell invasion. In contrast, 3D tissues benefit from large pores that promote cell infiltration and proliferation within the scaffold to form a bulk tissue [7–9].

Electrospinning has been widely used to create porous scaffolds due to its modest cost, and ability to create a range of pore sizes [3, 10–12]. This technique produces topographically-intense meshes of overlaid fibers with a high surface-area-to-volume ratio and interconnected tortuous pores. Although electrospun scaffolds may be appropriate for many 3D tissues, they are likely a poor choice for 2D tissues due to their highly-variable, heterogeneous pore size [13, 14]. Achieving a particular average pore size is far from trivial and involves a major refinement process to find the correct combination of six or more parameters which may be unique to a particular polymer and lab set-up. However, even after the appropriate *average* pore size has been achieved, the scaffold will still be at risk for cell invasion due to large pores that persist even when the average decreases because of a wide size distribution. For example, one study found that electrospun meshes with fibers 300 nm in diameter contained an average pore diameter of 5 μm, yet the maximum diameter was 30 μm, much larger than the size of most human cells [15]. In addition, 2D tissues can respond poorly to the intense topography of electrospun scaffolds that can further impede proper monolayer formation [16]. Unfortunately, other current scaffold fabrication methods other than electrospinning are similarly inappropriate for 2D applications because of their own set of inherent limitations, the most common of which are insufficient resolution and poorly-controlled pore size/tortuosity/location. As a result, fabrication techniques are typically chosen based on their ability to produce a scaffold that meets one or a subset of the most important design criteria for a particular application [17–20].

The need for additional scaffold fabrication techniques has long been recognized, but advances have typically been slow and incremental [20]. However, tissue engineers may be able to leverage existing technology from other fields to develop new scaffold fabrication techniques that lack the shortcomings of existing methods. Microfabrication is one such technology with the potential to revolutionize scaffold fabrication due to its fine control over micro- and nano-architecture [20–22]. Although most of the studies using microfabrication tools in the biomedical literature focus on topographically patterned surfaces [23–25], these tools also have the potential to produce porous scaffolds with exceptional control [26–30].

This article presents a novel scaffold fabrication technique hereafter referred to as pore casting. This method is capable of creating sub-micron pores in thin scaffolds with user-defined pore properties including size, shape, and location in a variety of materials. The closest predecessor to this technique was reported by Jackman et al. [29] which used a polydimethylsiloxane (PDMS) mold to induce pores in polymer films. While effective at producing large (100 μm) pores, the previous technique was incapable of producing small or high aspect ratio pores like those required for 2D tissues (<5 μm) due to poor PDMS stability and solvent incompatibility [29–32]. Pore casting looks to overcome these problems by replacing PDMS with non-deformable, solvent-friendly silicon to produce thin scaffolds with minimum topography and user-defined pore size. These scaffolds may be particularly attractive for the development of small-diameter vascular tissue engineering which has been stymied by thrombogenicity, loss of patency, and bursting [33–40].

2 Materials and methods

Pore casting employs photolithography, deep reactive ion etching (RIE), and spin-assisted templating to create thin, porous scaffolds. First, a computer-aided design program was used to design a photomask pattern of 2D features that would later be converted into a 3D feature. Though there are infinite combinations of patterns, shapes, and materials imaginable, this proof of concept example was used to produce high aspect ratio cylindrical pores in a thin poly(ε-caprolactone) (PCL) film.

2.1 Membrane supports

Costar 12-well transwells with 0.4 μm pores were purchased from Thermo Fisher Scientific (Cambridge, MA). Transwell membranes were removed from the supporting structure and replaced with electrospun or pore-cast PCL films that were attached using Silastic Medical Adhesive from Dow Corning (Midland, MI). Prior to cell culture, all materials were soaked in 70 % ethanol for 24 h and rinsed with PBS.

2.2 Electrospun scaffold fabrication

PCL (M_n 70,000–90,000) was used to produce electrospun scaffolds. First, PCL was dissolved in 5:1 chloroform: methanol to form a solution that was 12 % w/v polymer. This solution was then dispensed at 10 ml/h onto a slowly rotating and translating collector at a working distance of

12 cm using an applied voltage of 15 kV. Scaffold morphology was assessed using ImageJ (National Institutes of Health, Bethesda, MD) and Photoshop (Adobe Systems Incorporated, San Jose, CA) analysis of scanning electron microscopy (SEM) images. Briefly, surface pore size was estimated in the XY plane using images collected at 2 kV and 250×. This magnification was found to focus on approximately the top three fiber layers which correspond to approximately one cell diameter in depth. The threshold function was then used to create a binary discrepancy between fibers and pores for increased clarity. The modified image was then used to quantify individual pore sizes in pixels and subsequently area in square microns using a known scale. Finally, pore size was represented as the diameter of a circle with equivalent area for ease of comparison to pore-cast scaffolds. A total of 100 pores were counted across multiple areas to determine pore size. The "Oval Profile" plug-in with radial sums for directionality was used to measure electrospun fiber directionality as described elsewhere [41].

2.3 Pattern design

The photomask pattern was produced using L-Edit (Tanner EDA Software Tools, Monrovia, CA). The pattern consisted of a square array of circles 1 μm in diameter with 5 μm center-to-center spacing. Once completed, the design files were sent to Toppan Photomasks, Inc. (Santa Clara, CA) where they were printed as a quartz photomask with transparent circles on an opaque chrome background.

2.4 Photolithography

Photolithography was used to transfer the array of features from a 2D photomask onto a photoresist-covered silicon wafer suitable for RIE. 10 cm boron-doped silicon wafers with a 5,000 Å-thick surface layer thermally-grown silicon dioxide were purchased from University Wafer, Inc. (South Boston, MA). Once cleaned and inspected, the wafers were coated with a thin layer of HMDS to serve as an adhesion promoter using an EVG101 Advanced Resist Processing System (EV Group Inc., Albany, NY), baked at 90 °C on a hot plate for 1 min, and subsequently coated with ~3,000 Å of ma-N 2403 (Micro Resist Technology GmbH, Berlin, Germany)—a negative photoresist. Wafers were then soft baked at 100 °C on a hot plate for 1 min to remove excess solvent. After cooling, wafers were loaded one at a time beneath the patterned photomask under vacuum contact and exposed to deep ultraviolet light (220 nm) for a total dose of 260 mJ/cm^2. Photoresist exposed to light through transparent areas in the photomask was cross-linked, while areas of photoresist beneath opaque chrome remained uncross-linked. Uncross-linked photoresist was then removed by developing in a solution of 5:1 Microposit® MF®-319 (Shipley Company, Marlborough, MA): H_2O for 60 s and hard baked at 100 °C in an oven for 30 min.

2.5 Reactive ion etching

All RIE was performed on a STS ASE HRM (Surface Technology Systems, Newport, United Kingdom) utilizing inductively coupled plasma technology. First, a 4 min and 15 s standard RIE processes was run using a platen power of 130 W under a flow of 20 ml/min CHF_3 and 30 ml/min CF_4 at a pressure of 200 mTorr to etch regions of silicon dioxide not protected by overlying photoresist (the space between circles). A deep RIE procedure was then carried out for 74 cycles of alternating etch and passivation steps with each cycle contributing additional vertical etch depth. The etch step was set at 17 W platen power, 600 W ECR power, and a flow of 130 ml/min SF_6 with 13 ml/min O_2 for 8 s at 20 mTorr. The passivation step used 0 W platen power, 600 W ECR power, and a flow of 90 ml/min C_4F_8 for 5 s at 20 mTorr. After a sufficient etch depth had been achieved, the wafer was treated with oxygen plasma in a March Asher PX-250 (Nordson, Westlake, OH) for 10 min at 200 W and 150 mTorr to remove any remaining photoresist. The wafer was then placed in a buffered oxide etch (7:1 v/v of 40 % NH_4F in water to 49 % HF in water) for 8 min to strip the silicon oxide layer and thereafter cleaned using piranha solution (3:1 v/v of H_2SO_4 to 30 % H_2O_2) for 20 min.

2.6 Spin-assisted polymer templating

A polymer solution of 2:15 w/v PCL:dichloromethane was mixed vigorously for 3 h. Prior to polymer application, the wafer was treated with oxygen plasma in a March Asher for 20 min at 150 W to create a thin oxide layer and thereby increase surface hydrophilicity. The silicon mold was then coated with 10 ml of the PCL solution and rotated on a CE100 Spinner (Brewer Science, Rolla, MO) at 1,500 rpm for 30 s causing the polymer solution to thin and solidify on the mold. Next, the mold and adherent scaffold were place into an oven at 67 °C for 15 min to re-flow the polymer and allow for any local areas of heterogeneous thickness to resolve. After the wafer and adherent film passively cooled to room temperature (27 °C), they were placed in a March Asher and treated with oxygen plasma for 20 min at 200 W and 150 mTorr to remove polymer aggregation on the tips of features. Finally, the film was removed from the wafer by slow and careful peeling from the wafer edge using tweezers to grip the unpatterned regions of film. A subset of films had their thickness measured prior to removal using an Alpha Step 500 Profiler

(KLA-Tencor, Milpitas, CA). A summary of the pore casting process is depicted in Fig. 1.

2.7 Scanning electron microscopy

Silicon molds were imaged directly using a Hitachi S-3500N Scanning Electron Microscope (Gaithersburg, MD) with an accelerating voltage of 5.0 kV. For biological imaging, cells were first fixed in a solution of 0.1 M sodium cacodylate, 0.1 M sucrose, and 3 % glutaraldehyde for 24 h. The samples were then dehydrated by sequential soaking in 35, 50, 70, 95, and two 100 % ethanol treatments for 10 min each. Dehydration was completed by covering samples with hexamethyldisilazane (HMDS) which was allowed to evaporate in a chemical fume hood at room temperature. PCL films were then mounted on aluminum stubs using double-sided copper tape and sputtered with 10 nm gold–palladium alloy using a Cressington 108auto Sputter Coater (Watford, United Kingdom) to prevent surface charging.

2.8 In vitro cell culture

MDCK, a canine kidney epithelial cell line and Caco-2, a human epithelial colorectal adenocarcinoma cell line were purchased from ATCC (Manassas, VA). Primary human umbilical vein endothelial cells (HUVECs) were generously provided by Dr. Gimbrone's laboratory (Brigham and Women's Hospital, Boston, MA). All materials were coated with 300 µl of 1 µg/ml laminin in phosphate buffered saline (PBS) for 2 h prior to cell seeding to promote cell adhesion. MDCK cells were seeded at 100,000 cells/cm^2 and maintained in alpha-modified minimum essential media (Sigma-Aldrich, St. Louis, MO) with 10 % fetal bovine serum, 1 % GIBCO® GlutaMAX (Life Technologies, Carlsbad, CA), and 1 % penicillin/streptomycin (Lonza, Allendale, NJ) for 3 days. Caco-2 cells were seeded at 40,000 cells/cm^2 in alpha-modified minimum essential media with 20 % fetal bovine serum (Atlanta Biologicals, Norcross, GA), 1 % GlutaMAX, and 1 % penicillin/streptomycin. After 24 h the media was replaced with serum-free media of the otherwise same formulation. Thereafter cells were re-fed every 2–3 days with the serum-free media until culture was terminated after 7 days. HUVECs were seeded at 50,000 cells/cm^2 and maintained in EBM-2 (Lonza) with 20 % fetal bovine serum, EGM-2 SingleQuot (Lonza), 1 % GlutaMAX, and 1 % penicillin/streptomycin. Media was replaced 24 h after seeding and every 2–3 days thereafter until the culture was ended at day 14. All cells were used within five passages of receiving them from their source.

2.9 Cell plating efficiency

Cell plating efficiency was assessed by counting the number of non-adherent cells at 24 h. Media samples were collected from the bottom and top of transwells taking care not to disturb adherent cells and quantified using a Coutler Counter (Beckman Coulter, Danvers, MA). The non-adherent cell count was then compared to the initial number of cells seeded to obtain the percentage of adherent cells on each scaffold.

2.10 Transepithelial resistance

Transepithelial resistance (TER) is a well-established measure of tight junction formation in epithelium [42]. Prior

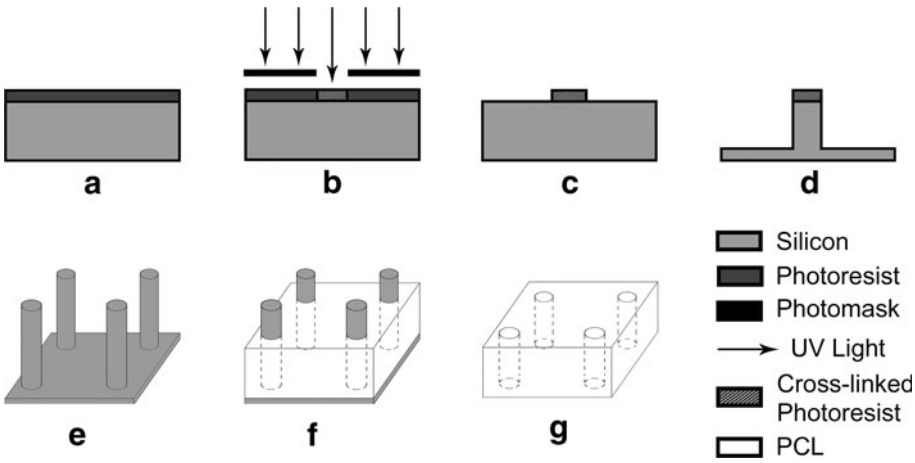

Fig. 1 Pore casting scaffold fabrication process. The surface of a surface-oxidized silicon wafer is **a** coated with photoresist and **b** exposed to deep UV light through a photomask for pattern transfer. **c** Unexposed photoresist is developed away yielding bare silicon that is subsequently **d** removed using deep RIE. **e** Remaining protective photoresist is then removed to produce a silicon master mold with cylindrical features. **f** A PCL solution is then deposited onto the mold as a thin layer using spin-assisted templating. **g** After solvent evaporation the film can be peeled from the mold to yield a porous polymeric scaffold

to cell seeding, a two-electrode TER instrument (World Precision Instruments, Inc., Sarasota, FL) was used to measure the basal electrical resistance of each scaffold. On the final day of culture, the process was repeated to measure electrical resistance of the cell-scaffold construct. The initial measurements for each scaffold prior to seeding were subtracted from the corresponding final cell-scaffold values to determine the cellular contribution to TER at each end point.

2.11 Immunohistochemistry

Upon completion of cell culture, cells were washed in PBS, fixed in 4 % paraformaldehyde for 10 min, and permeabilized in 0.1 % Triton X-100 for 10 min. Samples were then incubated in a blocking buffer of 2.5 % w/v bovine serum albumin and 3 % v/v goat serum in PBS at room temperature for 2 h. The sample was then submerged in blocking buffer containing 10 μl/ml of a primary antibody to zona occludin 1 (ZO-1), a tight junction-associated protein and incubated overnight on a shaker at 4 °C. The next day samples were washed with PBS and placed in blocking buffer with AlexaFluor 488 goat anti-rabbit green secondary antibody at 3.3 μl/ml and DAPI, a blue nuclear dye, at 10 μl/ml for 1 h. The samples were again washed with PBS and then incubated with AlexaFluor 594 phalloidin, a red stain for filamentous actin (f-actin), at 10 μl/ml for 20 min. After three additional washes with PBS the samples were cut, mounted on glass slides, and imaged using an Axioskop MOT 2 (Carl Zeiss Meditec, Inc., Dublin, CA).

2.12 Statistical analysis

Data was reported as mean ± standard deviation. In vitro results for adhesion and TER were analyzed with 8 independent replicates. Data sets were compared using a two-tailed unpaired Student's t test. A value of $P < 0.05$ was considered significant.

3 Results

3.1 Pore-cast scaffold characterization

After substantial refinement of the etching process, a mold of high aspect ratio cylinders with sub-micron diameter and near-perpendicular sidewalls was produced. After 74 cycles (~16 min process time) a feature height of 16.2 ± 0.2 μm was achieved. The diameter of the cylindrical features at the base and tip were 790 ± 50 and 680 ± 20 nm respectively (Fig. 2a) corresponding to a sidewall angle of 90.2°.

Films produced by spin-assisted templating PCL onto the silicon mold were 9.9 ± 0.3 μm thick which was less than the 16.2 μm feature height suggesting that pores fully transverse the scaffold. This observation was confirmed by SEM which showed cylinders protruding beyond the PCL surface during molding (Fig. 2b) and openings on both sides of the scaffold after delamination. Pore openings at the bottom (molded by the cylindrical base) and top of the film were 810 ± 60 and 650 ± 120 nm in diameter respectively (Fig. 2c, d). There was no significant difference between silicon feature diameter and pore size for the top ($P = 0.40$) or bottom ($P = 0.32$) of the scaffold. The total porosity of the scaffold was ~1.33 %.

3.2 Electrospun scaffold characterization

The electrospun scaffold properties were chosen based on handling (a practical requirement for surgical manipulation), inherent electrical resistance, and precedence in the literature [37, 43–47]. Electrospun scaffolds had baseline resistances of 5.2 ± 0.3 Ω/cm^2 which was statistically similar to the 6.7 ± 0.5 Ω/cm^2 of bare pore-cast scaffolds ($P = 0.06$). Electrospun scaffold morphology qualitatively appeared very different than pore-cast PCL (Fig. 3). Electrospun fibers were 3.68 ± 0.57 μm in diameter and resulted in surface-level pores 8.85 ± 4.40 μm across that were significantly larger than cast pores ($P < 0.001$). The scaffolds were also much thicker than pore-cast PCL at 246 ± 23 μm ($P < 0.001$). Fast Fourier transform analysis revealed that the scaffold did not display a preferred fiber orientation ($P = 0.84$).

3.3 Cell plating efficiency

24 h after seeding, 92.5 ± 2.5 % of MDCK cells were adherent to the electrospun scaffold compared to 97.1 ± 1.5 % on pore-cast scaffolds ($P < 0.001$). Caco-2 cells showed similar plating efficiencies on each material with 89.8 ± 1.5 % adherence on electrospun PCL compared to 89.8 ± 2.0 % on pore-cast scaffolds ($P = 0.96$). HUVECs also displayed statistically similar levels of adherence on each scaffolds with 97.1 ± 0.3 and 97.2 ± 0.6 % adhesion on electrospun and pore-cast PCL respectively ($P = 0.85$). These results are summarized in Fig. 4.

3.4 Assessment of cellular morphology by SEM

MDCK cells on electrospun scaffolds closely followed the shape of the underlying fibers and as a result, displayed 3D architecture (Fig. 5). Scaffold coverage appeared to be incomplete with poor coverage between widely-spread fibers. In addition, many cells with rounded morphology were present, especially just below the surface layer of fibers. Alternately, MDCK cells on pore-cast PCL completely covered the scaffold surface as a confluent

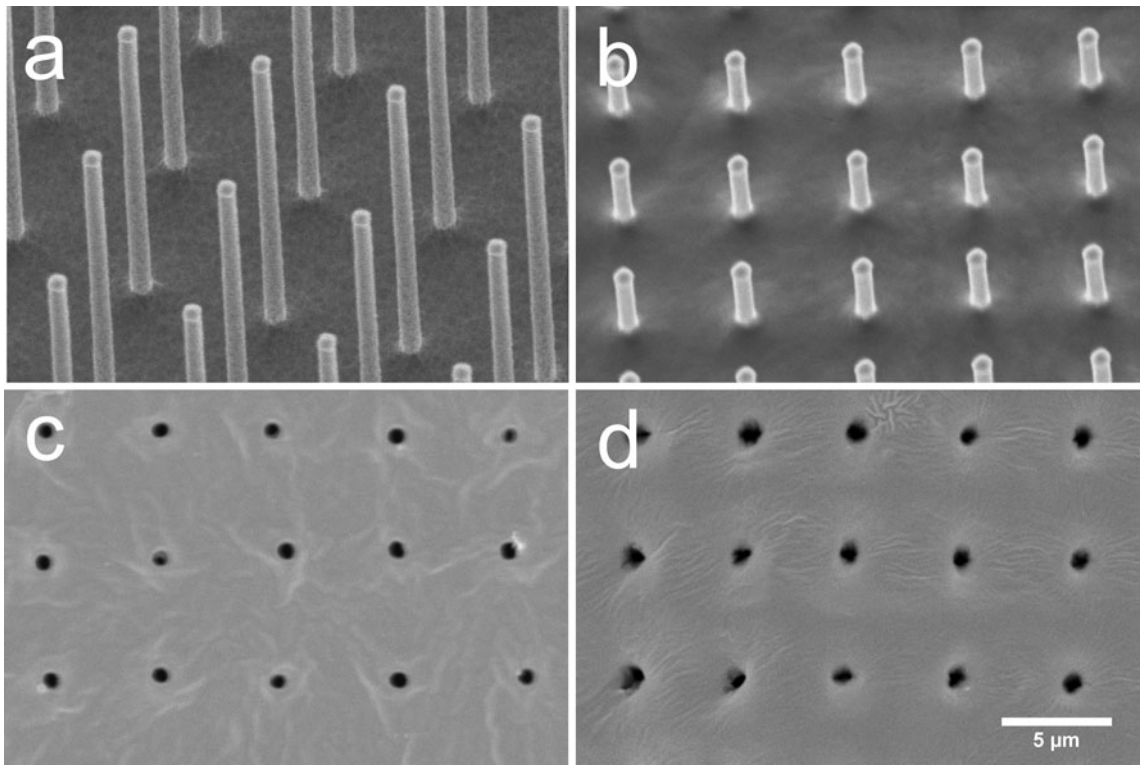

Fig. 2 Scanning electron microscopy images of the pore casting process. **a** Silicon mold with high aspect ratio vertical columns. **b** PCL spun onto the silicon mold. **c** *Top* and **d** *bottom* of pore-cast scaffold after removal from the mold

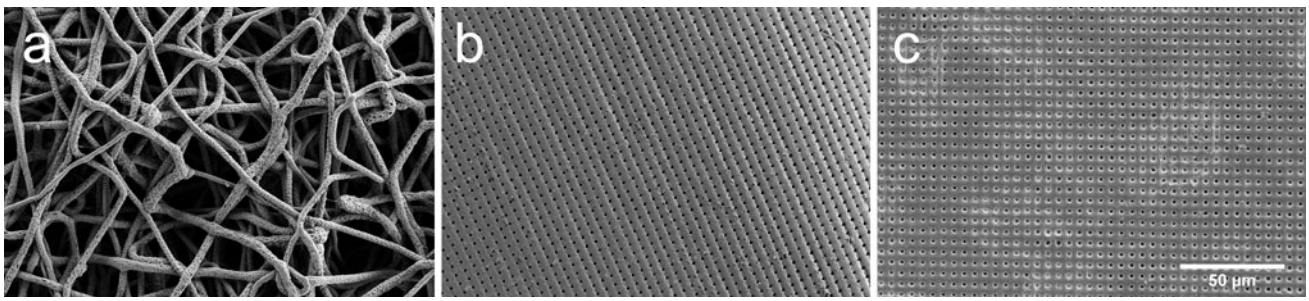

Fig. 3 Scanning electron microscopy images of **a** an electrospun mesh, **b** a pore-cast scaffold with circular pores ~700 nm in diameter, and **c** a pore-cast scaffold with circular pores ~1.5 μm in diameter. Scaffolds from **a** and **b** were used as substrates for cell culture in this study

monolayer with individual cells generally assuming a well-spread polygonal morphology (Fig. 5).

Caco-2 cells on electrospun PCL formed small islands separated by large areas of exposed scaffold. Cell coverage was poor even in the most densely populated regions (Fig. 5). Compared to MDCK, Caco-2 cells appeared more capable of spanning large pores. As a result, scaffold invasion was reduced, though still present in some areas. In contrast, Caco-2 cells on pore-cast scaffolds were well-spread, flat, and completely covered the surface as a confluent monolayer (Fig. 5).

HUVECs on electrospun PCL exhibited poor surface coverage and appeared suspended between fibers at the surface and several layers below. Cells also displayed numerous cell processes that extended to adjacent fibers and nearby cells. HUVECs on pore-cast scaffolds were confluent and well-spread with processes extended radially to adjacent cells (Fig. 5).

3.5 Cellular organization and tight junction formation

MDCK cells on electrospun scaffolds displayed virtually no ZO-1 localization at cell–cell borders, but stained intensely for f-actin in stress fibers centralized within dense clusters of cells (Fig. 6, row 1, asterisks). Cell nuclei appeared to deform around electrospun fibers and were visible in multiple focal planes indicating scaffold penetration. Alternately, MDCK on the pore-cast scaffold appeared to form a

monolayer of polygonal, flat, and well-distributed cells with centralized nuclei. ZO-1 was present in high levels at the cell–cell border indicating the proper localization of tight junctions (Fig. 6, row 2, arrowheads). All cell types including MDCK exhibited minimal f-actin staining on pore-cast scaffolds, so fluorescent intensity was increased using image processing techniques. After image enhancement, f-actin was found preferentially at the cell border indicating a cortical localization of microfilaments characteristic of mature epithelium.

Caco-2 cells on electrospun scaffolds showed generally poor epithelial morphology (Fig. 6, row 3). ZO-1 was localized at some cell–cell junctions, but lacking in many others. Cortical f-actin was also only observed in a small subset of cells. Like MDCK, Caco-2 cell nuclei were observed in multiple focal planes suggesting scaffold penetration and 3D tissue formation. Caco-2 cells on the pore-cast scaffold, however, formed a well-organized epithelium (Fig. 6, row 4). ZO-1 was localized at cell–cell borders and generally co-stained with f-actin. Cells were evenly spread across the surface of the scaffold and did not seem to overlap or deform due to scaffold architecture.

HUVECs were highly heterogeneous on electrospun PCL and displayed a fibroblastic morphology (Fig. 6, row 5). ZO-1 was diffuse and poorly enriched at cell borders. Numerous f-actin-positive stress fibers were also observed. Cells appeared to overlap in most locations, though sparse areas of monolayer were present. HUVECS on pore-cast PCL displayed normal epithelial morphology, with uniform cell shape and prominent membranous localization of both f-actin and ZO-1 (Fig. 6, row 6).

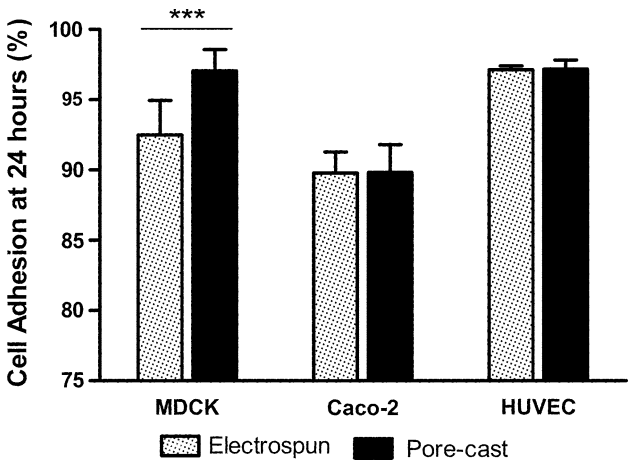

Fig. 4 Percentage adherent cells on electrospun (*gray*) and pore-cast (*black*) scaffolds 24 h after seeding. *** indicates $P < 0.001$

3.6 Barrier function

After 3 days of culture the resistance of MDCK cells on electrospun PCL reached $15 \pm 7\ \Omega/cm^2$ which was significantly lower than $381 \pm 84\ \Omega/cm^2$ on pore-cast scaffolds ($P < 0.001$). Caco-2 cells also exhibited significantly lower TER on electrospun PCL compared to pore-cast scaffolds measuring 5 ± 2 and $1{,}850 \pm 240\ \Omega/cm^2$ respectively after 7 days ($P < 0.001$). HUVECs achieved a minimal TER of $1 \pm 1\ \Omega/cm^2$ on electrospun PCL which was significantly lower than their resistance on pore-cast scaffolds of $13 \pm 2\ \Omega/cm^2$ ($P < 0.001$). A summary of these results is included in Table 1.

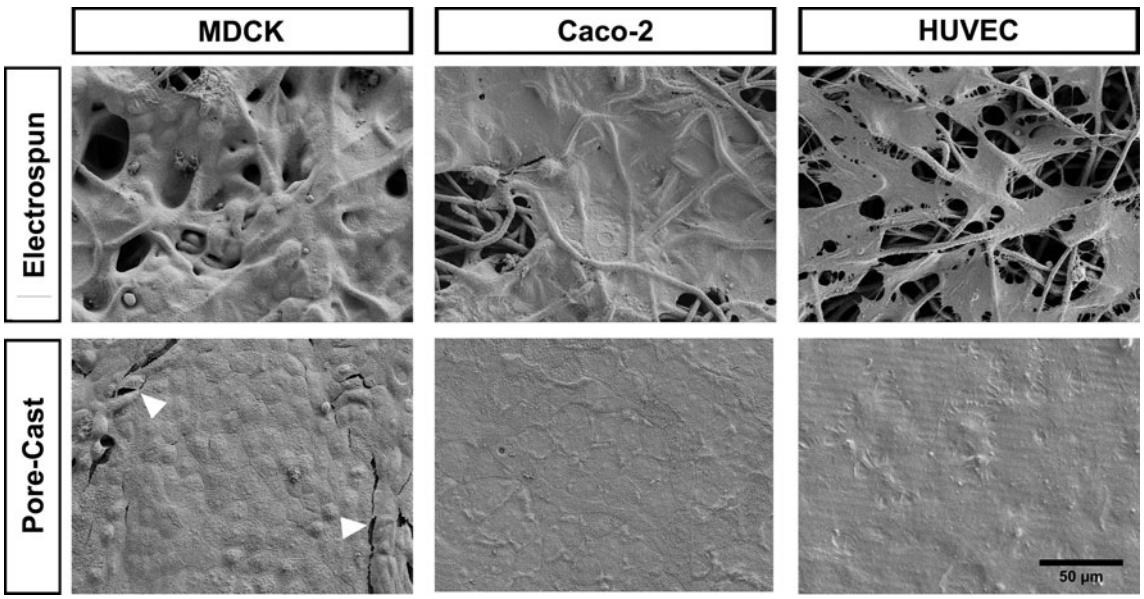

Fig. 5 SEM images of cells on electrospun and pore-cast PCL scaffolds. MDCK, Caco-2, and HUVEC cultured for 3, 7, and 14 days respectively. Cracking (*white arrowheads*) is an artifact of dehydration/fixation and not representative of cell morphology

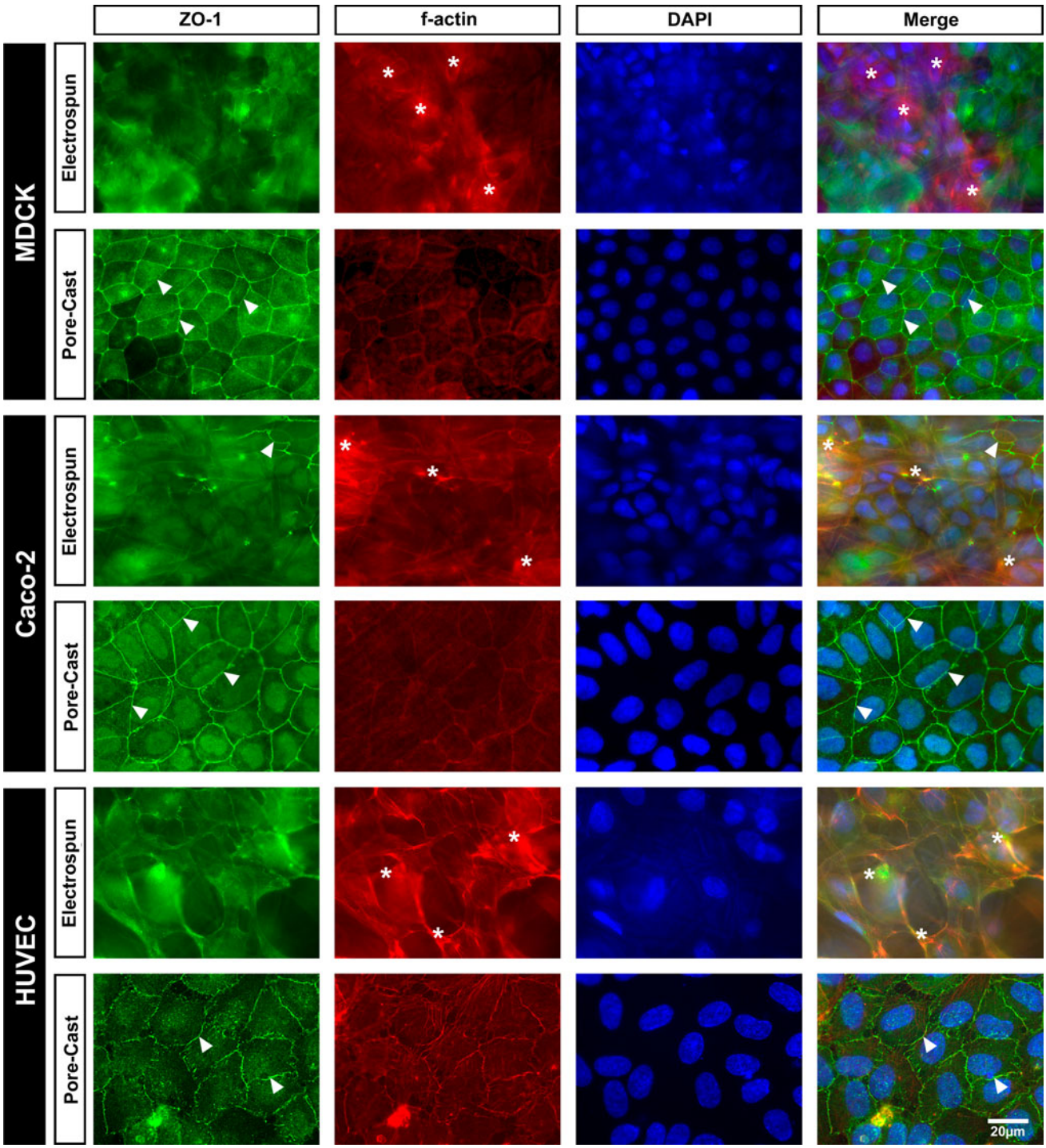

Fig. 6 Immunohistochemical staining of cells for ZO-1 (*green*, column 1), f-actin (*red*, column 2), DAPI (*blue*, column 3), and the merged imaged (column 4). MDCK, Caco-2, and HUVEC cultured for 3, 7, and 14 days respectively. Areas of cells enriched in stress fibers are indicated by an *asterisk*. *Arrowheads* indicate membranous ZO-1 localization. *Asterisks* indicate intense f-actin staining

4 Discussion

4.1 Scaffold characterization

Pore casting has the ability to produce thin film scaffolds with well-controlled pore size and location. Cylinders in the silicon mold were slightly smaller than the initial pattern on the photomask due to the small horizontal component of the deep RIE recipe used. Though deep RIE preferentially removes silicon in the vertical direction, slight undercutting may also occur, resulting in reduced feature size. Because the eventual pore size is well-correlated with mold feature

Table 1 Transepithelial resistance (Ω/cm^2) of scaffolds and cells

Scaffold	No cells	MDCK	Caco-2	HUVECs
Electrospun	5 ± 0	15 ± 7	5 ± 2	1 ± 1
Pore-cast	7 ± 1	381 ± 84***	1,850 ± 240***	13 ± 2***

Values are expressed as mean ± SD

*** $P < 0.001$ compared to same cell type on electrospun scaffold

diameter, photomask design should account for a slight decrease in feature diameter due to horizontal etching.

Due to the brittle nature of silicon, mold fracture during scaffold delamination is perhaps the greatest practical challenge in pore casting. As anticipated, high aspect ratio features were more prone to breaking than shorter or wider features. This scaffold was chosen as an extreme stress test to demonstrate the capabilities of pore casting for creating pores well below the size required to prevent epithelial cell transmigration. However, scaffolds with circular pores 1.5 μm in diameter (Fig. 3c) and rectangles 1.5 μm × 10 μm were also fabricated (data not shown). These larger features were easier to fabricate while likely sufficient to prevent epithelial cell transmigration.

The angle of the silicon features was absolutely critical in producing a scaffold that could be released from the mold without fracture. Though cylindrical features with 90° sidewall angles are optimal for maintaining a cylindrical pore, practical concerns regarding scaffold removal should also be considered. Features with larger tips than bases were fractured during scaffold delamination as slightly smaller pores produced by the narrower feature base were unable to deform around the wider mold tips. Much >90° features, though easily removed, produce conical pores that limit pore aspect ratio and spacing. In this case 90.2° features (base slightly wider than tip) provided a compromise that produced a scaffold with nearly-cylindrical pores that could also be removed from the mold. Although pore casting requires a more substantial initial effort to develop than the PDMS-based molding methods described by Jackman et al. [29] and Vozzi et al. [30], the 10- to 100-fold gain in minimum feature size is paramount in creating porous scaffolds appropriate for 2D tissue engineering. In addition, once an etching protocol has been established, subsequent patterns and molds can be created by repeating the process with a different photomask pattern, but otherwise using the same protocol, an advantage over electrospinning which requires a major redevelopment process.

Electrospun scaffolds design was chosen to match the TER of pore-cast scaffolds for subsequent comparison of cellular barrier function; however, matching this value resulted in obvious differences in scaffold morphology and pore size. Electrospun scaffolds appeared to have a generally rough surface topography and possessed pores that were both larger and more variable in size. Electrospun fiber diameter was similar to several previous studies that used these meshes for tissue engineering of small diameter vessels [43–45], though other reports use smaller fibers with an average diameter of 500–1,000 nm [37, 46, 47]. In any case, average fiber diameter alone is not fully-representative of scaffold morphology as it fails to describe the range of fiber sizes and pore size distribution which may be very broad [37, 48, 49].

4.2 Cell behavior

Cells on pore-cast scaffolds displayed improved morphology, surface coverage, monolayer formation, and barrier function compared to cells on electrospun meshes. Cell adhesion was similar or superior on pore-cast scaffolds and generally high for all conditions with a minimum of 89.8 % plating efficiency. As a result, it does not appear that adhesion should be a major deciding factor for scaffold selection. Instead, surface coverage and epithelial tissue architecture are likely more critical criteria for proper tissue function. Pore-cast scaffolds excelled in each of these areas as all three cell types appeared flat and either confluent or approaching confluency on pore-cast scaffolds. When seeded on electrospun scaffolds these same cells displayed poor surface coverage that would severely diminish an engineered tissue's barrier function. This would be particularly detrimental for engineered blood vessels where platelet aggregation on exposed biomaterial surfaces results in thrombosis and loss of patency [33–35]. Because both scaffolds had similar cell adhesion, this lack of coverage suggests that cells have migrated into the scaffold which is acceptable for 2D tissue formation. This conclusion was further supported by immunohistochemistry and SEM which revealed cells in spatial planes beneath the fibrous surface.

The minimum pore size conducive to cell infiltration varied by cell type, an observation that has been reported by other groups previously [50, 51]. The sub-micron pores contained in pore-cast scaffolds were sufficiently small to prevent epithelial and endothelial cell invasion and maintain a cell monolayer; however this was not the case for electrospun meshes. Caco2 cells displayed some ability to span the large pores present in the electrospun meshes, but MDCK and HUVECs migrated freely into the scaffold inducing a multi-layered tissue not characteristic of epithelium or endothelium. HUVEC invasion of electrospun scaffolds was especially surprising because a previous study had found that these cells attached and spread on 6 μm electrospun fibers at similar levels as on flat tissue culture polystyrene [43]. Thus, the smaller (3.67 μm) fibers were thought to have a similar morphological outcome, but

instead cells appeared stretched between fibers at and below the surface.

Immunohistochemistry revealed further differences between cells on electrospun and pore-cast PCL. Cells on electrospun scaffolds displayed heterogeneous and incomplete ZO-1 localization at cell–cell borders indicating that tight junction (barrier) formation was disrupted. However, cells on pore-cast scaffolds exhibited well-localized, continuous ZO-1 staining suggesting improved barrier function. This observation was quantitatively confirmed by TER which was significantly higher for all cell types on pore-cast PCL. Both MDCK and Caco-2 cells on pore-cast scaffolds quickly attained very high TER values indicating proficient epithelial barrier function. Although HUVECs on both scaffolds displayed a low resistance compared to the other cell types, this was expected for microvascular endothelial cells [52]. Cells on pore-cast scaffolds also displayed cortical f-actin localization which is characteristic of mature, well-formed epithelium [53]. Alternately, cells on electrospun PCL contained densely-packed stress fibers that are indicative of a challenged state.

In this experiment electrospun scaffolds inhibited the formation of a normal epithelial monolayer. This poor cell response would likely have been mitigated slightly by using smaller diameter fibers; however, small fibers are very difficult to fabricate. Determining the correct parameters for electrospinning requires substantial development effort in order to achieve sub-micron fibers with homogeneous diameter while avoiding "beading" which results in large polymer deposits along the fiber [54]. Despite numerous attempts, the authors were unable to fabricate electrospun PCL fibers that met this set of criteria. However, even if thin fibers had been successfully fabricated, large pores with the potential for invasion would still persist. Though decreasing fiber size decreases the spatial frequency of large pores, the randomness of electrospinning makes it statistically-probable that large openings would persist. Kwon et al. [15] observed that electrospun meshes with fibers as small as 300 nm in diameter resulted in an average and maximum pore diameter of 5 and 30 μm respectively. This large maximum pore size is especially concerning because any cell invasion is inappropriate for 2D tissues. Kwon's group also found that maximum pore size increased dramatically with even slight increases in fiber diameter. Increasing the average fiber diameter from 300 nm to just 1.16 μm corresponded to a new maximum pore size of 400 μm [15]. Because of this, there may be no ideal fiber size that achieves an appropriate balance of sufficient porosity and reliable prevention of cell invasion.

Track etched films represent another possible alternative to pore casting. Unlike electrospinning, track etching is able to create very uniform, exceptionally small pores down to 10 nm in a flat surface [55]. However, track etching possesses other limitations that are both fundamental and practical. The major inherent limitation of track etching is random pore location that can result in fused pores with double (or more) the pore diameter that may negatively affect the membrane's ability to prevent cell invasion. Further, from a practical perspective, track etched membranes require the use of machinery that is exceptionally rare and are only commercially available in a handful of polymers [55]. As a result, there is a major challenge in employing track etched membrane for tissue engineering which is likely to benefit from particular materials and tightly-regulated pore size.

In terms of practical fabrication advantages, pore casting requires only standard microfabrication tools, can be used to easily create morphologically identical porous scaffolds using different component materials, and minimizes the time required for changing pore architecture. These benefits offer flexibility in processing that is ideal for scientific research by using supremely-relevant controls for experimentation. For instance, using the same mold to create scaffolds of different materials allows the researcher to isolate the effect of material composition on cell behavior. Likewise, applying the same etching recipe to a different photomask pattern (pore size/spacing/shape) will allow researchers to isolate only the effects of pore architecture. In addition, pore casting also has several advantages over electrospinning and track etching including that the resulting pores are fully user defined in terms of both location and shape. Uniform, reproducible pores substantially reduce the variability between scaffolds and eliminate the possibility of larger pores that would be at risk for cell invasion. Further, pore shape could be co-opted to provide topographical cues such as alignment via contact guidance in order to improve engineered tissue organization. As a result, pore casting is uniquely positioned as an accessible and robust technique capable of creating porous scaffolds ideal for epithelial and endothelial cell culture.

5 Conclusions

Herein we describe a novel technique for the fabrication of porous thin film scaffolds. We then provide in vitro data demonstrating enhanced epithelial and endothelial cell behavior on these scaffolds compared to electrospun meshes. Perhaps the largest advantage offered by pore casting is its high degree of control which allows for complete control over pore size, shape, spacing, and location with sub-micron resolution. Though this proof-of-concept study demonstrates the fabrication of PCL films with $\sim$700 nm cylindrical pores, a variety of porous polymer films could be produced by spinning a different solution onto the same mold. In addition, pore architecture could also

be easily altered by designing a different photomask pattern, but employing the same etch recipe. In contrast to electrospinning and track-etching which require substantial process refinement when altering pore/fiber architecture and/or material, the flexibility of pore casting allows the user to easily create highly-controlled porous scaffolds. Pore casting has the potential to fill a currently unmet need by producing porous scaffolds appropriate for 2D tissue engineering. Pore-cast scaffolds may be particularly valuable for vascular tissue engineering, in which complete cell coverage, trans-scaffold transport, and mechanical properties are essential, but poorly regulated by current approaches.

Acknowledgments The authors would like to thank Stefan Yohe and Joe Hersey (Dept. of Biomedical Engineering, Boston University) for fabricating the electrospun PCL control materials and Dr. Gimbrone (Brigham & Women's Hospital) for HUVECs. This work was supported by the National Institutes of Health Director's New Innovation Award 1DP2OD006649 (MSG).

References

1. Carletti E, Motta A, Migliaresi C. Scaffolds for tissue engineering and 3D cell culture. Methods Mol Biol. 2011;695:17–39.
2. Dado D, Levenberg S. Cell-scaffold mechanical interplay within engineered tissues. Semin Cell Dev Biol. 2009;20:656–64.
3. McCullen SD, Ramaswamy S, Clarke LI, Gorga RE. Nanofibrous composites for tissue engineering applications. Wiley Interdiscip Rev Nanomed Nanobiotechnol. 2009;1:369–90.
4. Nikkhah M, Edalat F, Manoucheri S, Khademhosseini A. Engineering microscale topographies to control the cell-substrate interface. Biomaterials. 2012;33:5230–46.
5. Ashkenas J, Muschler J, Bissell MJ. The extracellular matrix in epithelial biology: shared molecules and common themes in distant phyla. Dev Biol. 1996;180:433–44.
6. Amini AR, Adams DJ, Laurencin CT, Nukavarapu SP. Optimally porous and biomechanically compatible scaffolds for large-area bone regeneration. Tissue Eng Part A. 2012;18:1376–88.
7. Hutmacher DW. Scaffold design and fabrication technologies for engineering tissues—state of the art and future perspectives. J Biomater Sci Polym Ed. 2001;12:107–24.
8. Sachlos E, Czernuszak JT. Making tissue engineering scaffolds work. Review: the application of solid freeform fabrication technology to the production of tissue engineering scaffolds. Eur Cell Mater. 2003;5:29–40.
9. Zhang R, Ma PX. Synthetic nano-fibrillar extracellular matrices with predesigned macroporous architectures. J Biomed Mater Res. 2000;52:430–8.
10. Pham QP, Sharma U, Mikos AG. Electrospinning of polymeric nanofibers for tissue engineering applications: a review. Tissue Eng. 2006;12:1197–211.
11. Prabhakaran MP, Ghasemi-Mobarakeh L, Jin G, Ramakrishna S. Electrospun conducting polymer nanofibers and electrical stimulation of nerve stem cells. J Biosci Bioeng. 2011;112:501–7.
12. Di Martino A, Liverani L, Rainer A, Salvatore G, Trombetta M, Denaro V. Electrospun scaffolds for bone tissue engineering. Musculoskelet Surg. 2011;95:69–80.
13. Nisbet DF, Forsythe JS, Shen W, Finkelstein DI, Horne MK. Review paper: a review of the cellular response on electrospun nanofibers for tissue engineering. J Biomater Appl. 2009;24:7–29.
14. Soliman S, Sant S, Nichol JW, Khabiry M, Traversa E, Khademhosseini A. Controlling the porosity of fibrous scaffolds by modulating the fiber diameter and packing density. J Biomed Mater Res A. 2011;96:566–74.
15. Kwon IK, Kidoaki S, Matsuda T. Electrospun nano- to microfiber fabrics made of biodegradable copolyesters: structural characteristics, mechanical properties and cell adhesion potential. Biomaterials. 2005;26:3929–39.
16. Schindler M, Nur-E-Kamal A, Ahmed I, Kamal J, Liu HY, Amor N, Ponery AS, Crockett DP, Grafe TH, Chung HY, Weik T, Jones E, Meiners S. Living in three dimensions: 3D nanostructured environments for cell culture and regenerative medicine. Cell Biochem Biophys. 2006;45:215–27.
17. Desai TA. Micro- and nanoscale structures for tissue engineering constructs. Med Eng Phys. 2000;22:595–606.
18. Yang S, Leong KF, Du Z, Chua CK. The design of scaffolds for use in tissue engineering. Part I. Traditional factors. Tissue Eng. 2001;7:679–89.
19. Patel H, Bonde M, Srinivasan G. Biodegradable polymer scaffold for tissue engineering. Trends Biomater Artif Organs. 2011;25:20–9.
20. Lu L, Mikos AG. The importance of new processing techniques in tissue engineering. MRS Bull. 1996;21:28–32.
21. Valmikinathan CM, Hoffman J, Yu X. Impact of scaffold micro and macro architecture on Schwann cell proliferation under dynamic conditions in a rotating wall vessel bioreactor. Mater Sci Eng C Mater Biol Appl. 2011;31:22–9.
22. Del Gaudio C, Grigioni M, Bianco A, De Angelis G. Electrospun bioresorbable heart valve scaffold for tissue engineering. Int J Artif Organs. 2008;31:68–75.
23. Andersson AS, Bäckhed F, von Euler A, Richter-Dahlfors A, Sutherland D, Kasemo B. Nanoscale features influence epithelial cell morphology and cytokine production. Biomaterials. 2003;24:3428–36.
24. Flemming RG, Murphy CJ, Abrams GA, Goodman SL, Nealy PF. Effects of synthetic micro- and nano-structured surfaces on cell behavior. Biomaterials. 1999;20:573–88.
25. Teixeira AI, Abrams GA, Bertics PJ, Murphy CJ, Nealy PF. Epithelial contact guidance on well-defined micro- and nanostructured substrates. J Cell Sci. 2003;116:1881–92.
26. Carletti E, Endogan T, Hasirci N, Hasirci V, Maniglio D, Motta A, Migliaresi C. Microfabrication of PDLLA scaffolds. J Tissue Eng Regen Med. 2011;5:569–77.
27. Sodha S, Wall K, Redenti S, Klassen H, Young MJ, Tao SL. Microfabrication of a three-dimensional polycaprolactone thin-film scaffold for retinal progenitor cell encapsulation. J Biomater Sci Polym Ed. 2011;22:443–56.
28. Figallo E, Flaibani M, Zavan B, Abatangelo G, Elvassore N. Micropatterned biopolymer 3D scaffold for static and dynamic culture of human fibroblasts. Biotechnol Prog. 2007;23:210–6.
29. Jackman RJ, Duffy DC, Cherniavskaya O, Whitesides GM. Using elastomeric membranes as dry resists and for dry liftoff. Langmuir. 1999;15:2973–84.
30. Vozzi G, Flaim C, Ahluwalia A, Bhatia S. Fabrication of PLGA scaffolds using soft lithography and microsyringe deposition. Biomaterials. 2003;24:2533–40.
31. Delamarche E, Schmid H, Michel B, Biebuyck H. Stability of molded polydimethylsiloxane microstructures. Adv Mater. 1997;9:741–6.
32. Qin D, Xia Y, Whitesides GM. Soft lithography for micro- and nanoscale patterning. Nat Protoc. 2010;5:491–502.
33. McBane JE, Sharifpoor S, Labow RS, Ruel M, Suuronen EJ, Santerre JP. Tissue engineering a small diameter vessel substitute: engineering constructs with select biomaterials and cells. Curr Vasc Pharmacol. 2012;10:347–60.
34. McGuigan AP, Sefton MV. The influence of biomaterials on endothelial cell thrombogenicity. Biomaterials. 2007;28:2547–71.

35. Yang J, Motlagh D, Webb AR, Ameer GA. Novel biphasic elastomeric scaffold for small-diameter blood vessel tissue engineering. Tissue Eng. 2005;11:1876–86.
36. Lee SJ, Liu J, Oh SH, Soker S, Atala A, Yoo JJ. Development of a composite vascular scaffolding system that withstands physiological vascular conditions. Biomaterials. 2008;29:2891–8.
37. Thomas V, Donahoe T, Nyairo E, Dean DR, Vohra YK. Electrospinning of Biosyn(®)-based tubular conduits: structural, morphological, and mechanical characterizations. Acta Biomater. 2011;7:2070–9.
38. Williams C, Xie AW, Yamato M, Okano T, Wong JY. Stacking of aligned cell sheets for layer-by-layer control of complex tissue structure. Biomaterials. 2011;32:5625–32.
39. Wu H, Fan J, Chu CC, Wu J. Electrospinning of small diameter 3-D nanofibrous tubular scaffolds with controllable nanofiber orientations for vascular grafts. J Mater Sci Mater Med. 2010; 21:3207–15.
40. Khan OF, Sefton MV. Endothelialized biomaterials for tissue engineering applications in vivo. Trends Biotechnol. 2011;29: 379–87.
41. Ayres CE, Jha BS, Meredith H, Bowman JR, Bowlin GL, Henderson SC, Simpson DG. Measuring fiber alignment in electrospun scaffolds: a user's guide to the 2D fast Fourier transform approach. J Biomater Sci Polym Ed. 2008;19:603–21.
42. Wegener J, Abrams D, Willenbrink W, Galla HJ, Janshoff A. Automated multi-well device to measure transepithelial electrical resistance under physiological conditions. Biotechniques. 2004;37: 590–7.
43. Heath DE, Lannutti JJ, Cooper SL. Electrospun scaffold topography affects endothelial cell proliferation, metabolic activity, and morphology. J Biomed Mater Res A. 2010;94:1195–204.
44. Del Gaudio C, Fioravanzo L, Folin M, Marchi F, Ercolani E, Bianco A. Electrospun tubular scaffolds: on the effectiveness of blending pol(ε-caprolactone) with poly(3-hydroxybutyrate-co-3-hydroxyvalerate). J Biomed Mater Res B Appl Biomater. 2012;100B:1883–98.
45. Wang X, Heath DE, Cooper SL. Endothelial cell adhesion and proliferation to PEGylated polymers with covalently linked RGD peptides. J Biomed Mater Res A. 2012;100:794–801.
46. Zhang M, Wang K, Wang Z, Xing B, Zhao Q, Kong D. Small-diameter tissue engineered vascular graft made of electrospun PCL/lecithin blend. J Mater Sci Mater Med. 2012;23:2639–48.
47. Hajialai H, Shahgasempour S, Naimi-Jamal MR, Peirovi H. Electrospun PGA/gelatin nanofibrous scaffolds and their potential in vascular tissue engineering. Int J Nanomed. 2011;6:2133–41.
48. Hsia HC, Nair MR, Mintz RC, Corbett SA. The fiber diameter of synthetic bioresorbable extracellular matrix influences human fibroblast morphology and fibronectin matrix assembly. Plast Reconstr Surg. 2011;127:2312–20.
49. Vaquette C, Cooper-White JJ. Increasing electrospun scaffold pore size with tailored collectors for improved cell penetration. Acta Biomater. 2011;7:2544–57.
50. McMillan JR, Akiyama M, Tanaka M, Yamamoto S, Goto M, Abe R, Sawamura D, Shimomura M, Shimizu H. Small-diameter porous poly(epsilon-caprolactone) films enhance adhesion and growth of human cultured epidermal keratinocyte and dermal fibroblast cells. Tissue Eng. 2007;13:789–98.
51. Salem AK, Stevens R, Pearson RG, Davies MC, Tendler SJB, Roberts CJ, Williams PM, Shakesheff KM. Interactions of 3T3 fibroblasts and endothelial cells with defined pore features. J Biomed Mater Res. 2002;61:212–7.
52. Wegener J, Zink S, Rösen P, Galla HJ. Use of electrochemical impedance measurements to monitor β-adrenergic stimulation of bovine aortic endothelial cells. Pflügers Arch. 1999;437:925–34.
53. Vasioukhin V, Bauer C, Yin M, Fuchs E. Directed actin polymerization is the driving force for epithelial cell–cell adhesion. Cell. 2000;100:209–19.
54. Fong H, Chun I, Reneker DH. Beaded nanofibers formed during electrospinning. Polymer. 1999;40:4585–92.
55. Apel P. Track etching technique in membrane technology. Radiat Meas. 2001;34:559–66.